Chemical Engineering Journal 160 (2010) 873–881

Contents lists available at ScienceDirect

Chemical Engineering Journal

journal homepage: www.elsevier.com/locate/cej

Mass transfer during Taylor flow in microchannels with and without chemical reaction

N. Shao, A. Gavriilidis, P. Angeli*

Department of Chemical Engineering, University College London, Torrington Place, London WC1E 7JE, UK

ARTICLE INFO

Article history:
Received 24 July 2009
Received in revised form 8 December 2009
Accepted 24 February 2010

Keywords:
Taylor flow
Mass transfer
Microchannel
Chemical reaction
CO_2 absorption

ABSTRACT

The characteristics of mass transfer from gas to liquid during Taylor flow in capillaries with diameter less than 1 mm with and without chemical reaction were investigated with Computational Fluid Dynamics modelling using 5 vol.% CO_2/N_2 mixture and 0.2 M NaOH or water as the gas and liquid phases, respectively. The effects on mass transfer of chemical reaction and of bubble velocity, bubble geometry and capillary size were studied. For the simulations a unit cell was used (a Taylor bubble and a liquid slug) with periodic boundary conditions at the inlet and the outlet of the unit cell, while the CO_2 concentration at the gas–liquid interface was dynamically updated to reflect the decreasing amount of CO_2 in the gas phase. The numerical model was able to predict well experimental data on the chemical absorption of CO_2 in a NaOH solution. The mass transfer performance for the various cases studied was evaluated using the CO_2 absorption fraction $X\%$ (the percentage of CO_2 transferred from the gas to the liquid phase) and the liquid utilization index Ψ (mole of CO_2 absorbed per unit volume of NaOH). Both these parameters were significantly higher in the case of chemical absorption compared to the physical one. The volumetric mass transfer coefficients, k_La, for the physical absorption were found to vary between 0.3 and 1.5 s^{-1} in line with literature values for Taylor flow but higher than in normal gas–liquid contactors while the specific areas achieved varied between 1000 and 10,000 m^2/m^3. Interestingly, for the conditions investigated, k_La was found to increase with channel size as did $X\%$ during physical absorption. The absorption fraction, however, increased with decreasing channel size when reaction was present. When reaction was present, CO_2 absorption was found to be enhanced between 3 and 12 times compared to physical absorption.

1. Introduction

Gas–liquid two-phase flow in microchannels has been the subject of increased research interest in the past few years [1–3]. It is encountered in many important applications, such as miniature heat exchangers, microscale process units, research nuclear reactors, materials processing and thin film deposition technology, biotechnology systems and potential space applications. One of the most common two-phase flow patterns in microchannels is Taylor flow that consists of elongated bubbles with equivalent diameter usually many times that of the channel diameter, separated by liquid slugs. The bubbles adopt a characteristic capsular shape and can either completely or nearly completely fill the channel cross-section where at most a thin liquid film separates them from the channel wall. A significant advantage of Taylor flow is the large gas–liquid interfacial area, which improves interfacial mass transfer; this feature becomes more important as the size of the microchannel decreases [4]. In addition, the improved radial mixing because of the recirculation patterns that appear in the liquid [5] enhances mass transfer within the liquid slugs [6] while the separation of the bulk liquid by the bubbles significantly reduces axial mixing [7]. As a result, Taylor flow has attracted a lot of attention and its characteristics have been discussed in a large number of publications, e.g. Kreutzer et al. [8], Garstecki et al. [9], and Haverkamp et al. [10].

The characterisation of mass transfer during Taylor flow is necessary for the design of microreactors that operate under this flow regime. A number of investigators have attempted to calculate the mass transfer coefficients for physical gas absorption. Irandoust et al. [11] studied experimentally oxygen absorption into water, ethanol and ethylene glycol and used penetration theory and the correlation by Clift et al. [12] to develop a model for mass transfer that included contributions from the bubble cap and from the film side of the bubble to the liquid. A correction factor needed to be applied to match the theoretically derived k_La with the experimental data while the results indicated that both bubble caps and the film side of the bubble contributed to mass transfer. Berčič and Pintar [13] studied methane absorption in water and developed an equation for the mass transfer coefficient using a CSTR by-pass model (Eq. (1)). k_La was found to depend on slug length only, which

* Corresponding author. Tel.: +44 20 7679 3832; fax: +44 20 7383 2348.
E-mail address: p.angeli@ucl.ac.uk (P. Angeli).

1385-8947/$ – see front matter © 2010 Elsevier B.V. All rights reserved.
doi:10.1016/j.cej.2010.02.049

Nomenclature

a	specific area (m^2/m^3)
A	interfacial area (m^2)
C	concentration (mol/l)
C^*	interfacial concentration (mol/l)
d	diameter (m)
D	diffusivity (m^2/s)
F	mole flowrate (kmol/s)
h	parameter
He	Henry's constant kmol/(m^3/atm)
I	ionic strength (kmol/m^3)
k	reaction rate constant (m^3/(kmol s))
k_L	liquid side mass transfer coefficient (mol/s)
l	reactor length (m)
P	pressure (atm)
Q	volumetric flowrate (m^3/s)
r	reaction rate
R	gas constant (0.082 m^3 atm/(K kmol))
t	time (s)
T	temperature (K)
U	velocity (m/s)
U_G,, U_L	superficial gas and liquid velocities (m/s)
$\bar{u}$	velocity (m/s)
V	volume (m^3)
x	radial coordinate (m)
$X\%$	CO_2 absorption fraction
z	axial coordinate (m)

Greek symbols

μ	dynamic viscosity (Pa s)
ρ	density (kg/m^3)
σ	surface tension (N/m)
δ	film thickness (m)
Ψ	liquid utilization (mol CO_2/ml NaOH solution)
ε	volume fraction (-)

Dimensionless numbers

Ca	capillary number, $Ca = \mu_L U_B/\sigma$
Re_G	superficial gas Reynolds number, $Re_G = \rho_G U_G d_H/\mu_G$
Re_L	superficial liquid Reynolds number, $Re_L = \rho_L U_L d_H/\mu_L$
Sc_L	liquid Schmidt number, $Sc_L = \mu_L/\rho_L D_{CO_2(L)}$
Sh_L	liquid Sherwood number, $Sh_L = k_L d_H/D_{CO_2(L)}$

Subscripts

B	bubble
cap	bubble caps
CO_2	related to carbon dioxide
CO_3^{2-}	related to carbonate
film	film region
G	gas
H	hydraulic
i	chemical species
L	liquid
OH^-	related to hydroxide
S	slug
UC	unit cell
vol	volume

can probably be attributed to the relatively large bubble lengths (overall unit cell length is up to 0.22 m) used in the study where the film becomes quickly saturated and unable to contribute further to gas absorption. A Computational Fluid Dynamics (CFD) study for mass transfer in capillaries under Taylor flow was carried out by van Baten and Krishna [5], who confirmed that both the bubble caps and the film side of the bubble contribute to mass transfer. A correlation was developed for $k_L a$ (Eq. (2) after modification by [14]) using penetration theory which compared favourably with the CFD results. For rather short unit cells (with most $L_{UC} < 0.025$ m) Vandu et al. [14] developed a $k_L a$ correlation (Eq. (3)) based on the $k_{L,film}$ suggested by van Baten and Krishna [5] where a value of C_1 of 4.5 fitted best the experimental data of air absorption in water in 1–3 mm diameter capillaries of circular and square cross-sections. For short contact times, i.e. short bubble length at the same bubble velocity, mass transfer was found to be a function of channel dimension (Eqs. (2) and (3)). Yue et al. [15] investigated CO_2 physical and chemical (into $NaHCO_3/Na_2CO_3$ buffer solution and NaOH solution) absorption in a rectangular microchannel ($d_H = 667\,\mu m$) and derived a correlation for the mass transfer coefficient under slug flow (Eq. (4)).

$$k_L a = 0.111 \frac{(U_G + U_L)^{1.19}}{((1-\varepsilon_G)L_{UC})^{0.57}} \tag{1}$$

$$k_L a = k_{L,cap} a_{cap} + k_{L,film} a_{film} = 2\frac{\sqrt{2}}{\pi}\sqrt{\frac{DU_B}{d}}\frac{4}{L_{UC}} + \frac{2}{\sqrt{\pi}}\sqrt{\frac{DU_B}{\varepsilon_G L_{UC}}}\frac{4\varepsilon_G}{d} \tag{2}$$

$$k_L a = C_1 \sqrt{\frac{DU_G}{L_{UC}}}\frac{1}{d_H} \tag{3}$$

$$Sh_L \cdot a \cdot d_H = 0.084 Re_G^{0.213} Re_L^{0.912} Sc_L^{0.5} \tag{4}$$

The above studies reveal that many parameters, such as bubble velocity, bubble length, slug length, unit cell length and capillary size, affect mass transfer in Taylor flow. However, there are no parametric studies reported when chemical reaction is also present, despite the common use of Taylor flow in applications that involve reactions.

In this paper, parametric studies on the mass transfer during CO_2 absorption into aqueous alkaline solutions with and without reaction under Taylor flow in microchannels are carried out numerically. This particular system is chosen because it involves a fast reaction that would particularly benefit from the improved mass transfer in microchannels but is also very relevant industrially in applications such as CO_2 removal from synthesis gas [16], CO_2 removal from flue gases [17] and some environmental applications [18]. The simple and periodic morphology of the Taylor bubbles and the laminar flow characteristics in microchannels make the system suited to investigations by Computational Fluid Dynamics (CFD) simulations. Numerical simulations are particularly beneficial for carrying out parametric studies because the effects of the different parameters can be easily isolated, which is not always possible with experiments (for example, in this case bubble length from slug length). There have been a few CFD studies on Taylor flow, e.g. on hydrodynamics [19,20], on bubble formation [21,22] and on mass transfer without reaction [5,23]. In the approach by van Baten and Krishna [23] the liquid domain was only modelled while the Taylor bubble was treated as a void and a constant tracer concentration was applied at the gas–liquid interface to solve the mass transfer. When reaction is present, however, this modelling approach will lead to physically incorrect CO_2 absorption fractions, i.e. >100%, because the CO_2 amount is continuously supplied from the gas and consumed by the reactant in the liquid. The correct interfacial CO_2 concentration is therefore necessary to solve the problem.

A CFD model is formulated in this study for mass transfer in Taylor flow where both the gas and the liquid domains are solved so that the interfacial CO_2 concentration is varied during the simulation. The effect of a fast reaction on mass transfer is initially considered. This is followed by parametric studies on the effect on mass transfer and mass transfer coefficient of the flow geometry such as bubble length, slug length and unit cell length and of the channel dimension. These results would help to design Taylor flow microreactors with improved performance.

2. Model formulations

2.1. Reaction system

CO_2 absorption into aqueous alkaline solutions is an intrinsically very fast and homogeneous reaction [24], making it a suitable system to study in small channels. The absorption follows the steps:

$$CO_{2(G)} \leftrightarrow CO_{2(L)} \tag{i}$$

$$CO_{2(L)} + OH^- \leftrightarrow HCO_3{}^- \tag{ii}$$

$$HCO_3{}^- + OH^- \leftrightarrow CO_3{}^{2-} + H_2O \tag{iii}$$

The overall reaction can be written as

$$CO_{2(L)} + 2OH^- \leftrightarrow CO_3{}^{2-} + H_2O$$

Step (i) represents the process of physical dissolution of gaseous CO_2 into the liquid solution. As the rate of this process is comparatively very high, the equilibrium at the interface can be described by Henry's law:

$$C^*_{CO_2(L)} = HeP_{CO_2} \tag{5}$$

where $C^*_{CO_2(L)}$ is the equilibrium concentration of carbon dioxide at the gas–liquid interface, P_{CO_2} is the partial pressure of CO_2 in the gas phase and He is the equilibrium solubility of CO_2 in the liquid phase. The value of He can be calculated using Eq. (6) [25], where C_i and h_i are the concentration and a parameter characteristic to each ion in the solution, while h_G is the absorbed gas in the liquid phase. The values of h_i and h_G are given by Schumpe [25]. At 293 K, the equilibrium solubility of CO_2 in water is 0.039 kmol/(m^3 atm).

$$\log\left(\frac{He}{He_{water}}\right) = -\sum_i (h_i + h_G)C_i \tag{6}$$

Reaction (iii) is an ionic reaction whose rate is significantly higher than that of reaction (ii). Therefore, reaction (ii) governs the overall rate of the process and follows second-order kinetics [26]:

$$r = -k_{OH^-}C_{OH^-}C_{CO_2(L)} \tag{7}$$

The equilibrium constant of reaction (ii) at ambient temperature is about 6×10^7 m^3/K mol [27] and it can be considered as practically irreversible. The rate constant k_{OH^-} for reaction (ii) was given by Pohorecki and Moniuk [26] as:

$$\log(k_{OH^-}) = 11.916 - \frac{2382}{T} + 0.221I - 0.016I^2 \tag{8}$$

The solution ionic strength, I, can be calculated from the ion concentration C and its valence z for the various ions present (Eq. (9)):

$$I = 0.5\sum_i C_i z_i{}^2 \tag{9}$$

The reaction rate can be calculated by solving simultaneously Eqs. (5)–(9) [28].

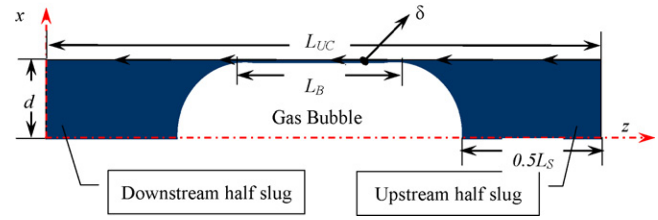

Fig. 1. Geometry and boundaries of the computational domain.

2.2. CFD model formulation

In the model development it is assumed that gravity, surface tension gradient (Marangoni effect) and gas compressibility have negligible effects. The bubble is assumed to have a cylindrical body with spherical caps at the ends for the low Capillary numbers encountered in this study ($Ca < 10^{-3}$) [29], as shown in Fig. 1. The bubble volume decrease due to CO_2 absorption is assumed to be negligible because of the small initial concentration of CO_2 (5 vol.%). The solution domain consists of two sub-domains, depicted in Fig. 1 by the white and shaded areas, representing the gas and the liquid, respectively. By solving both phases, the CO_2 concentration at the gas–liquid interface is dynamically updated. The governing equations are the Navier–Stokes and continuity equations for the liquid phase velocity field (Eqs. (10) and (11)), convection–diffusion equation for the liquid phase mass transfer (Eq. (12)) and diffusion equation for the gas phase mass transfer (Eq. (13)). Initial simulations showed that convection in the gas phase can be omitted because of the large CO_2 diffusivity in the gas that leads to small CO_2 concentration gradients. The reaction term in Eq. (12) refers to both reactants as shown in Eqs. (14) and (15).

$$\rho_L\frac{\partial\bar{u}}{\partial t} + \nabla\cdot(\rho_L\bar{u}\bar{u} - \mu_L(\nabla\bar{u} + (\nabla\bar{u})^T)) = -\nabla P \tag{10}$$

$$\nabla\cdot\bar{u} = 0 \tag{11}$$

$$\frac{\partial}{\partial t}C_i + \nabla\cdot(\bar{u}C_i - D_i\nabla C_i) = \begin{cases} r_i \\ 0 \end{cases} \tag{12}$$

where

r_i is used for the reaction scenario with i = CO_2(L) and OH^-; 0 is used for the physical absorption scenario

$$\frac{\partial}{\partial t}C_{CO_2(G)} + \nabla\cdot(-D_{CO_2(G)}\nabla C_{CO_2(G)}) = 0 \tag{13}$$

$$r_{CO_2(L)} = -k_{OH^-}C_{OH^-}C_{CO_2(L)} \tag{14}$$

$$r_{OH^-} = -2k_{OH^-}C_{OH^-}C_{CO_2(L)} \tag{15}$$

The simulations were carried out in the two-dimensional domain using axisymmetric cylindrical coordinates, in which the bubble was kept stationary while the wall moved with the bubble velocity in the direction opposite to the flow. For the boundary conditions of the hydrodynamic equations, the axial and radial velocity at the outer tube wall were set to $u_z = -U_B$ and $u_x = 0$, respectively where z and x are the axial and radial coordinates. Along the bubble surface, free slip boundary was used, i.e. $d\bar{u}/dn = 0$ where $d\bar{u}$ is the velocity component in the direction of the bubble surface and n is the normal direction to the bubble surface. For the mass transfer equations, along the bubble surface Henry's law was used to take into account the discontinuous concentration of CO_2 in the gas and liquid phases. Periodic boundary conditions were applied to the front and the back of the computational domain for velocity, pressure and concentrations, assuming that the inlet to the liquid slug is taken equal to the outlet. This assumption is only correct when the mass transferred during a time step is very small. van Baten and

Table 1
Parameters used in the simulated cases. T = 298 K, atmospheric pressure, $y_{CO_2,in}\% = 5\%$, $C_{NaOH,in}$ = 0.2 M, t = 0.05 s.

d [mm]	U_B [m/s]	L_S mm	L_B [mm]	L_{UC} [mm]	δ [μm]	$V_B \times 10^{10}$ m^3	$V_{UC} \times 10^{10}$ m^3	ε_B	$A \times 10^{-6}$ m^2	a [m^2/m^3]	k_La [s^{-1}]	E_t = 0.05s
0.5	**0**	0.26	0.25	1	5	1.09	1.96	0.554	1.14	5800	0.68	10.7
0.5	**0.01**	0.26	0.25	1	5	1.09	1.96	0.554	1.14	5800	0.93	7.5
0.5	**0.05**	0.26	0.25	1	5	1.09	1.96	0.554	1.14	5800	1.41	4.9
0.5	**0.1**	0.26	0.25	1	5	1.09	1.96	0.554	1.14	5800	1.49	4.6
0.5	0.05	0.26	**2**	2.75	5	4.39	5.40	0.813	3.83	7100	0.86	8.9
0.5	0.05	0.26	**5**	5.75	5	10.0	11.3	0.89	8.45	7490	0.52	11.6
0.5	0.05	**2**	0.25	2.74	5	1.09	5.38	0.202	1.14	2120	0.73	3.4
0.5	0.05	**5**	0.25	5.74	5	1.09	11.3	0.097	1.14	1010	0.35	3.5
0.5	0.05	0.443	0.5	**1.43**	5	1.56	2.81	0.554	1.53	5420	1.30	9.6
0.5	0.05	1.54	2	**4.03**	5	4.39	7.92	0.554	3.83	4840	0.83	5.0
0.25	0.05	2.12	1.63	4	2	1.09	1.96	0.554	1.83	9330	0.86	7.1

Bold numbers indicate the cases that are compared.

Krishna [23] reported that error from this assumption was at most 0.03%.

The equations were solved using a commercial finite element software (Comsol Multiphysics 3.3a). A free mesh with triangular elements was used, while along the bubble interface the mesh was refined to capture the steep concentration gradient in that region. Simulations were carried out in an Intel Pentium CPU processor with 3.20 GHz, 2.0 GB of RAM and the operating system was Windows XP x64 edition. Sensitivity studies on time step showed that a time step equal to 0.01 s was satisfactory, i.e. there was little concentration discrepancy when a smaller time step, e.g. 0.005 s, was used. Standard 2nd order elements were used for the velocity fields, 1st order elements for the pressure field and 3rd order elements for the mass transfer. The simulations were initially run in a steady-state mode to solve hydrodynamics in the liquid domain. The converged velocity field was then used as a starting point to solve the mass transfer in the liquid and in the gas domains simultaneously. Mass transfer was solved transiently to represent Taylor bubble movement downstream the reactor. Sensitivity analysis showed that the grid size should be less than 20 μm in the subdomains and <2 μm along the gas–liquid interface to achieve CO_2 absorption fraction independent of grid size.

2.3. Simulation conditions

Taylor flow was investigated in tubes ≤1 mm in diameter with bubble and slug lengths ranging from 0.5d to 10d based on previous experimental findings. The geometric characteristics of Taylor flow and the volume fraction for each scenario are listed in Table 1. The study is carried out at atmospheric pressure and 298 K. 0.2 mol/l NaOH or water is used as liquid phase and 5 vol.% CO_2/N_2 mixture as gas phase. These values are chosen so that the model assumption of negligible gas volume change due to CO_2 absorption is satisfied and there is enough liquid reactant ($F_{NaOH}/F_{CO_2} > 10$) even under the highest gas to liquid volume ratio in the reaction scenario. The liquid phase properties are taken equal to those of water, i.e. density ρ_L = 1000 kg/m^3, viscosity μ_L = 0.001 Pa s, for both physical and chemical absorption. Although the presence of NaOH is expected to affect the viscosity of the liquid phase and perhaps recirculation, as will be discussed later, the recirculation in the liquid does not play an important role in mass transfer. Therefore, the use of water properties in the chemical absorption case is not going to affect the trends observed. The diffusivities of CO_2 and of NaOH in the liquid phase are calculated by using Eqs. (16) and (17) [28]. Mass transfer in the different cases was compared through CO_2 absorption fraction, X%, defined as the percentage of CO_2 transferred from the gas to the liquid phase at time t, as shown in Eq. (18), where vol is the volume of the grid (using the option of computing volume values for axisymmetric modes) and V_G is the bubble volume that remains constant during the simulation. One drawback in using absorption fraction to assess mass transfer is that large absorption fractions can be achieved in an uneconomic way, e.g. by using a large amount of liquid reactant. To assess the performance of the reactor in each case, a liquid utilization index, Ψ, defined by Eq. (19) [28] is also used for comparison. In Eq. (19), the gas to liquid volumetric flowrate ratio can be substituted by the bubble volume fraction using Eq. (20) [30], which can be calculated from the Taylor flow geometric information (Table 1). Because the liquid volume has been taken into account in the equation, the interfacial area A will be used for comparisons hereafter where appropriate rather than the specific area. A residence time t of 0.05 s was selected for all simulations that ensured that in all cases the CO_2 absorption fraction was less than 100% while there were still significant differences between the various cases in each parametric study.

For physical absorption, a plug flow model was used to estimate the mass transfer coefficient k_La (Eq. (21)) from the simulations, where the ratio of liquid superficial velocity U_L to bubble velocity U_B can be obtained from Eqs. (20) and (22) [30]. An enhancement factor at time t, E_t (Eq. (23)) is also calculated in each case to compare the CO_2 chemical absorption with the physical one.

$$D_{CO_2(L)} = 1.97 \times 10^{-9}(1 - 0.129C_{OH^-} - 0.261C_{CO_3^{2-}}) \tag{16}$$

$$D_{NaOH(L)} = 1.7D^{1.35} \tag{17}$$

$$X\% = \left(1 - \frac{\sum_{i,\text{gasdomain}} \text{vol}_i C_{CO_2(G),t}/V_G}{C_{CO_2(G),0}}\right)\% \tag{18}$$

$$\Psi = \frac{F^{In}_{CO_2} - F^{Out}_{CO_2}}{Q^{In}_L} = \frac{F^{In}_{CO_2} X_{CO_2}}{Q^{In}_L} = \frac{Q^{In}_G}{Q^{In}_L} C^{In}_{CO_2} X_{CO_2} = \frac{\varepsilon_B}{1 - 0.61Ca^{0.33} - \varepsilon_B} C^{In}_{CO_2} X_{CO_2} \tag{19}$$

$$\varepsilon_B = \frac{U_G}{U_B} \tag{20}$$

$$k_La = \frac{U_L}{l} \ln \frac{C^* - C_{CO_2(L),in}}{C^* - C_{CO_2(L),out}} = \frac{U_L}{U_B t} \ln \frac{C^* - C_{CO_2(L),0}}{C^* - C_{CO_2(L),t}} = \frac{1 - 0.61Ca^{0.33} - \varepsilon_B}{t} \ln \frac{C^* - C_{CO_2(L),0}}{C^* - C_{CO_2(L),t}} \tag{21}$$

$$U_B = \frac{1}{1 - 0.61Ca^{0.33}} U_{TP} \tag{22}$$

$$E = \left(\frac{\Delta N_{CO_2(L),\text{chemical}}}{\Delta N_{CO_2(L),\text{physical}}}\right)_t = \frac{N_{CO_2(L),0} - N_{CO_2(L),t,\text{chemical}}}{N_{CO_2(L),0} - N_{CO_2(L),t,\text{physical}}} \tag{23}$$

Table 2
Experimental conditions and the derived geometric values used in simulations for model validation. T = 293 K, atmospheric pressure, $y_{CO_2,in}\% = 23\%$, $C_{NaOH,in}$ = 0.2 M, $C_{HCl,in}$ = 0.2 M.

d_H [mm]	l [mm]	Q_G [ml/min]	Q_L [μl/s]	L_{UC} [mm]	L_B [mm]	δ [μm]	α [m²/m³]	X%, experiment	X%, simulation
0.577	15	1.407	5	20.88	16.64	3.684	5638	44.60	49.20
0.577	15	1.407	20	9.63	4.63	4.835	3676	70.80	69.93
0.577	20	1.407	5	20.88	16.64	3.684	5638	53.95	56.05
0.577	20	1.407	20	9.63	4.63	4.835	3676	80.32	79.35
0.577	25	1.407	5	20.88	16.64	3.684	5638	58.02	61.50
0.577	25	1.407	20	9.63	4.63	4.835	3676	82.13	85.88
0.577	40	1.407	5	20.88	16.64	3.684	5638	72.98	77.00
0.577	40	1.407	20	9.63	4.63	4.835	3676	89.13	95.65
0.345	20	1.407	10	10.276	6.87	4.316	7918	64.82	70.63
0.345	20	1.407	20	7.304	3.61	5.077	6068	68.09	68.92
0.577	20	1.407	10	13.583	8.95	4.088	4788	67.16	72.12
0.577	20	1.407	20	9.632	4.63	4.835	3676	80.52	79.36
0.816	20	1.407	10	16.804	10.97	3.749	3404	58.23	57.09
0.816	20	1.407	20	11.900	5.61	4.444	2616	76.24	80.59

3. Results and discussion

3.1. Model validation

The model developed in Section 2.2 is validated against experimental data obtained in a similar system. The experiments were carried out at atmospheric pressure and a constant temperature of 292 K. The microchannels were fabricated on acrylic sheets using an engraving machine (Roland EGX-400) and bonded through diffusion bonding. The microchannel cross-section was of trapezium shape, which corresponded to the cutter tip profile. In the inlet the gas feed was smoothly flanked between two identical liquid feed channels. The gas mixture of nitrogen and carbon dioxide (CO_2 23 vol.%) was regulated with a Bronkhorst EL-FLOW F-110C mass flow controller for flows between 0.01 and 1 ml/min. The liquid phase, 0.2 M sodium hydroxide solution, was regulated through a Mili-Gat pump (0–6 ml/min). At the end of the absorption channel the fluids separated by gravity in a separator chamber. A quenching hydrochloric acid stream was introduced in the separation chamber to terminate the reaction by consuming the remaining NaOH. This was found to effectively reduce further adsorption in the separation chamber from 29% to below 0.77%. The CO_2 volume fraction before and after absorption, $y_{CO_2,in}$ and $y_{CO_2,out}$, respectively was analyzed with gas chromatography, from which the absorption fraction, X%, was obtained (Eq. (24)). The bubble and slug lengths used in the CFD simulations, were based on experimental measurements while the film thickness was calculated using Eq. (25) [31] from experimental operating conditions. These data along with the experimental and numerical CO_2 absorption fractions are given in Table 2.

$$X\% = \frac{\left(y_{CO_2,in} - y_{CO_2,out}\right)}{\left(1 - y_{CO_2,out}\right) y_{CO_2,in}}\% \tag{24}$$

$$\delta = \frac{0.66 Ca^{2/3}}{1 + 3.33 Ca^{2/3}} d_H \tag{25}$$

From the comparisons shown in Fig. 2, it can be seen that the simulations predict well the experiments and can therefore be used for the parametric investigations of the current study. The small discrepancy could be attributed to the differences between the experimental (trapezium) and numerical (circular) channel cross-section. In addition, the initial high CO_2 concentration would have resulted in the experiment in a decrease in the bubble volume and consequently the interfacial area which is not taken into account in the simulations. The larger interfacial area used in the simulations would explain the slightly higher CO_2 absorption fractions found numerically compared to the experiments.

3.2. Effects of fluid flow and chemical reaction

Three scenaria, mass transfer in a static system (diffusion only, U_B = 0 m/s), mass transfer with flow and mass transfer with flow and fast reaction present (CO_2 absorption into NaOH), are compared to show the effects on absorption fraction and liquid utilization of recirculation in the slugs of Taylor flow and of chemical reaction. The simulations are performed for three bubble velocities, 0.01, 0.05 and 0.1 m/s and the results are shown in Fig. 3. In the physical absorption scenaria, the utilization index, Ψ, and absorption fraction, X, are found to be larger in the cases with flow than in the static system and to increase with bubble velocity because at higher U_B the recirculation frequency is increased which improves mixing in the slug. However, the increase in X and Ψ with U_B becomes less significant from U_B > 0.05 m/s. It is expected that mass transfer between the bubble and the slug will be more significant in the first recirculation of the liquid in the slug when there is still no CO_2 in the liquid and a large concentration difference exists between the interface and the liquid. Interfacial mass transfer is expected to be less efficient in the following recirculations of the liquid when there will already be CO_2 in the liquid phase, particularly close to the interface, and the concentration gradient, necessary for the mass transfer, is reduced compared to the initial recirculation cycle. For the residence time examined (0.05 s), the number of recirculations in the liquid for bubble velocities of 0.01, 0.05 and 0.1 m/s is about 0.5, 2.5 and 5, respectively (the recirculation path is approximately $2(L_S + d/2)$ in these calculations). For U_B = 0.01 m/s the first recirculation cycle is not complete and the mass transfer performance

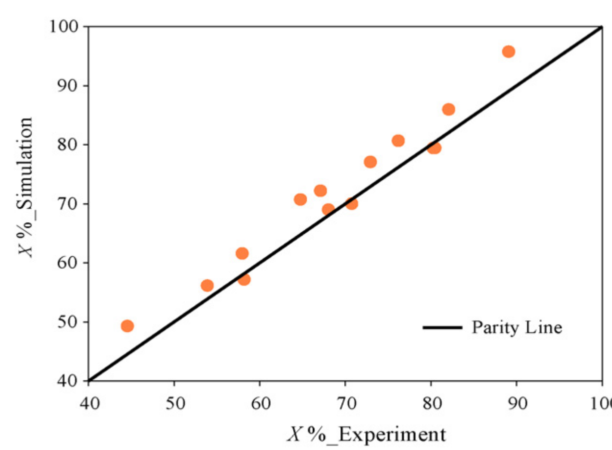

Fig. 2. Comparison of CO_2 absorption fraction between simulated and experimental results. For both experiments and simulations: channel (hydraulic) diameters = 0.345–0.816 mm, l = 15–40 mm, t = 0.06–0.52 s.

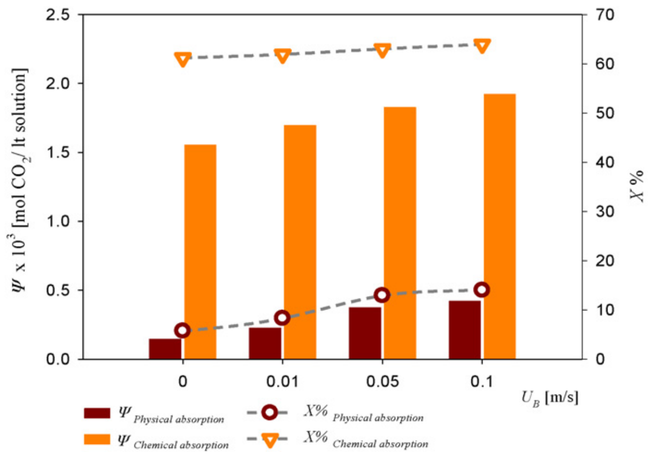

Fig. 3. Effect of bubble velocity on liquid utilisation index and CO_2 absorption fraction. $d = 0.5$ mm, $L_S = 0.26$ mm, $L_B = 0.25$ mm, $L_{UC} = 1$ mm, $\delta = 5$ µm, $t = 0.05$ s.

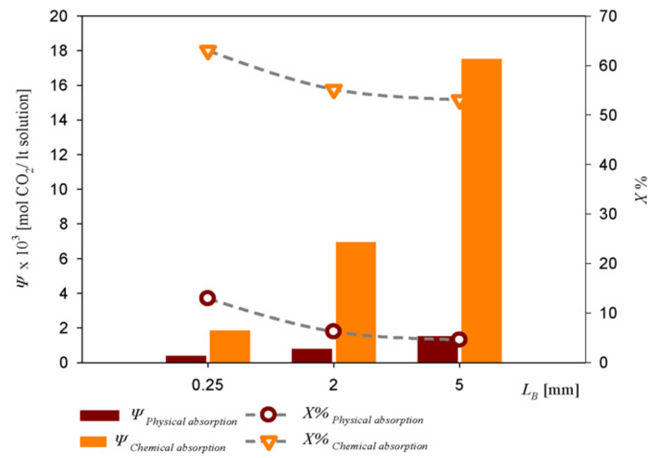

Fig. 4. Effect of bubble length on liquid utilization index and CO_2 absorption fraction. $d = 0.5$ mm, $U_B = 0.05$ m/s, $L_S = 0.26$ mm, $L_{UC} = 1$ mm, $\delta = 5$ µm, $t = 0.05$ s.

can be improved by increasing the recirculation frequency, which is achieved by increasing U_B (Fig. 3). Since the first recirculation is the most effective, any further increase in U_B does not improve significantly the mass transfer (see Fig. 3) despite the increase in the recirculation frequency.

The utilization index and absorption fraction are significantly improved in the presence of reaction (Fig. 3) because in this case the absorbed CO_2 in the liquid is converted, thus maintaining the CO_2 concentration difference between gas and liquid necessary to drive the mass transfer. However, when reaction is present, bubble velocity and liquid circulation have only a small effect on X or Ψ. The results in Fig. 3 show that compared to the static scenaria, X increases by 145% at $U_B = 0.1$ m/s in the physical absorption scenaria while the increase is only 5% in the reaction scenaria. The small improvement in the reaction scenaria with bubble velocity is probably due to the better mixing in the liquid slug that allows more concentrated NaOH to approach the gas–liquid interface. Although bubble velocity has a minor effect on liquid utilization in the reaction scenaria, higher bubble velocity at the same residence time means longer reactor, which is not appealing in terms of reactor cost.

The values of the mass transfer coefficient, k_La, for physical absorption and the absorption enhancement factor, E, when a chemical reaction is present are shown in Table 1. It can be seen that k_La increases with bubble velocity (see Table 1). Examples of CO_2 concentration in the gas and liquid phases are given in Table 3. Within the liquid slugs, there are concentration gradients in the physical absorption case while during chemical absorption there is no CO_2 which explains the higher mass transfer in this case. The concentration gradients in the gas phase are very small in both physical and chemical absorption. The lack of symmetry in the physical absorption case seems to reflect the direction of the velocity.

3.3. Effects of bubble length

By increasing the bubble length, the interfacial area of the bubble is increased together with the amount of CO_2 available in the gas phase for transfer. The mixing in the liquid bulk and the amount of NaOH remain the same due to the same slug size. It can be seen (Fig. 4) that longer bubbles lead to significantly higher utilization index in both scenaria, which is attributed to two phenomena: larger gas to liquid volume or flowrate and larger interfacial area. As a result more CO_2 can transfer to the liquid within a certain time and react with NaOH. The utilization index is increased by 858% when bubble length extends from 0.25 to 5 mm in the reactive case, but only by 300% during physical absorption probably because in this case the interface becomes quickly saturated with CO_2 and further mass transfer is slowed down. The absorption fraction, on the other hand, for both scenaria shows a decrease with L_B. This is because the increased amount of CO_2 that is transferred is offset by the larger amount of CO_2 present in the gas with increasing L_B. From Table 1 it can be seen that the mass transfer coefficient, k_La, also decreases with bubble length. Although the specific area per unit volume, a, increases, in longer bubbles the film becomes saturated with CO_2 and the film size part of the bubble does not contribute further to mass transfer.

3.4. Effects of slug length

The reactor performance for various slug lengths is shown in Fig. 5, which demonstrates that short slugs significantly improve the liquid utilization index for both scenaria because of the reduced amount of liquid used, i.e. reduced gas to liquid volume (Table 1). In contrast in both scenaria, the CO_2 absorption fraction decreases or remains the same with decreasing slug length as shown in Fig. 5. In the reaction scenaria there is hardly any change in X because the bubble interfacial area available for mass transfer does not change while the amount of NaOH is in all cases in excess. The change in absorption fraction is more noticeable in the physical absorption scenaria particularly when comparing $L_S = 0.26$ mm with the longer slugs. In the short slug more than one recirculation cycles

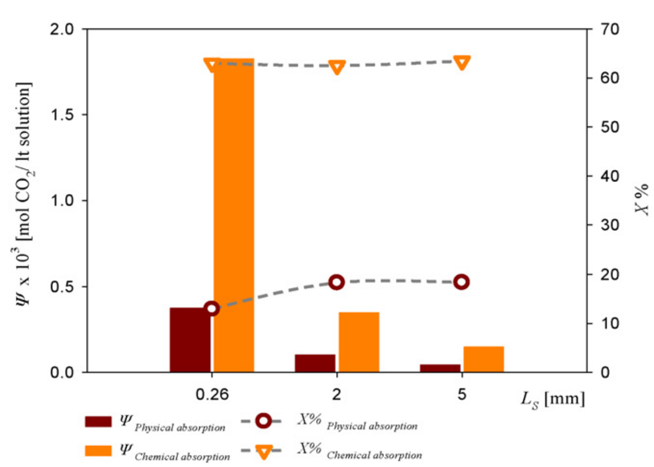

Fig. 5. Effect of slug length on liquid utilization index and CO_2 absorption fraction. $d = 0.5$ mm, $U_B = 0.05$ m/s, $L_B = 0.25$ mm, $L_{UC} = 1$ mm, $\delta = 5$ µm, $t = 0.05$ s.

Table 3
CO_2 concentration profiles. d = 0.25 mm, L_S = 0.26 mm, L_B = 0.25 mm, L_{UC} = 1 mm, δ = 5 μm, U_B = 0.05 m/s, t = 0.05 s.

	Physical absorption	Chemical absorption
$C_{CO2(G)}$	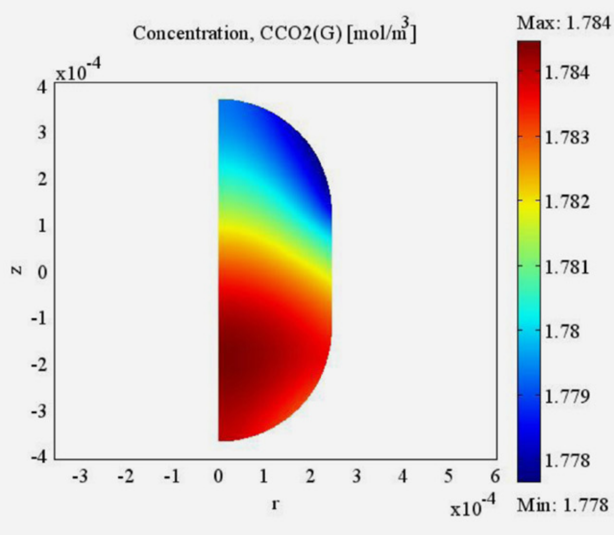 bubble	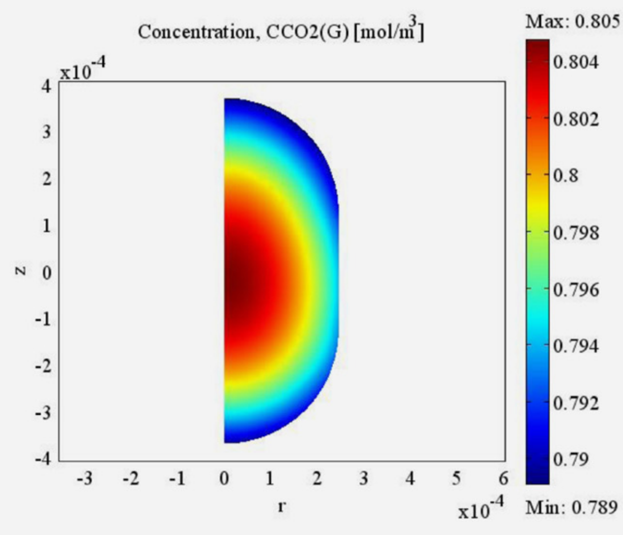 bubble
$C_{CO2(L)}$	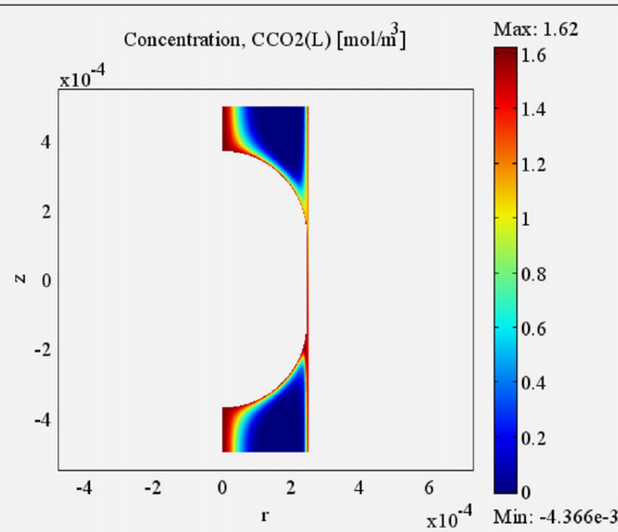 liquid slug	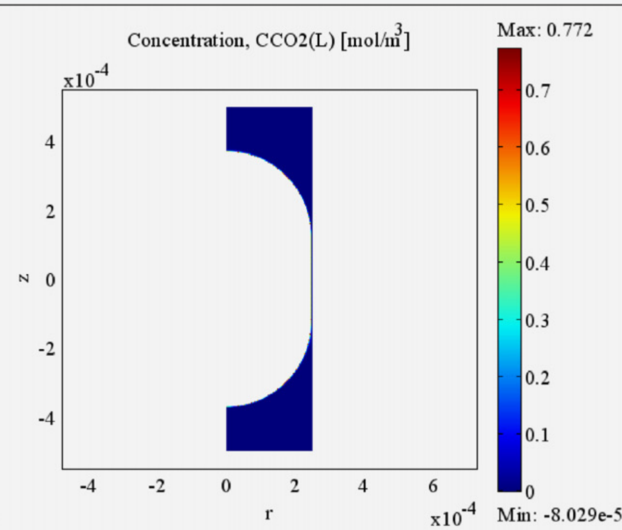 liquid slug

take place within the residence time while in the long ones (L_S = 2 and 5 mm) the first recirculation cycle is not complete which means that for the entire time of the simulation fresh liquid with no CO_2 comes in contact with the interface. The mass transfer coefficient, k_La, decreases with slug length following the reduction in specific area (see Table 1).

3.5. Effects of unit cell length

Bubble and slug lengths were found to be dependant on the inlet geometry [32]. In this section the unit cell length is varied and with this the bubble and slug lengths in order to maintain the same gas to liquid volume ratio (ε_B), see Table 1.

As can be seen in Fig. 6, Ψ decreases with increasing L_{UC} for both the reaction and the physical absorption scenaria. Since ε_B remains the same, the only parameter that can affect Ψ is CO_2 absorption fraction (Eq. (19)). For both scenaria, the amount of CO_2 increases with increasing unit cell size as larger bubbles are present. In addition, the interfacial area also increases that would improve mass transfer (Table 1) but at a lower rate than the bubble volume. For example, the interfacial area increases by 336% when L_{UC} changes from 1 mm to 4 mm, while the respective increase in bubble volume is 403%. The overall result is a lower absorption fraction in the longer unit cell length for both chemical and physical absorption (Fig. 6). In the physical absorption case, the first recirculation cycle in the slug takes longer time in a longer unit cell (longer slugs), which would have improved the mass transfer (see discussion in Section 3.2). However, this improvement in mass transfer does not balance the increased amount of CO_2 present and the absorption fraction is still lower than in the shorter unit cells. From Table 1 it can be seen that k_La decreases moderately with unit cell size in accordance with the decrease in specific area.

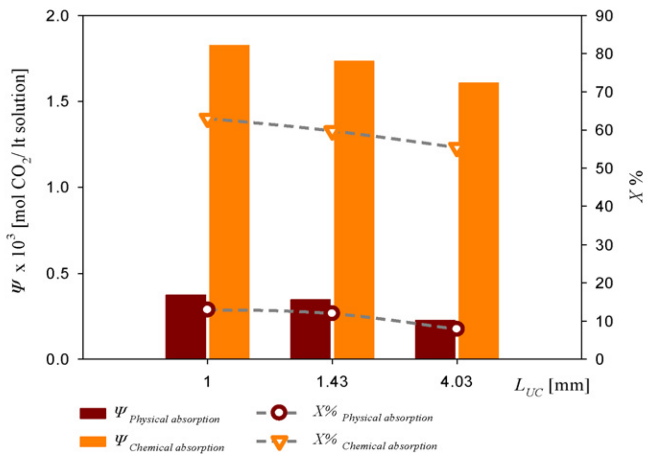

Fig. 6. Effect of unit cell length on liquid utilization index and CO_2 absorption fraction. $d = 0.5$ mm, $U_B = 0.05$ m/s, $\varepsilon_B = 0.554$, $\delta = 5$ µm, $t = 0.05$ s.

3.6. Effects of channel dimension

To investigate the effect of channel size on mass transfer, a channel size of 0.25 mm is used in addition to the 0.5 mm channel studied before. In order to keep the unit cell volume constant in the two channels, the unit cell length is extended in the 0.25 mm channel by four times which means longer bubbles and slugs. The bubble and slug lengths are adjusted so that the gas to liquid volume ratio remains the same in the two cases (see Table 1). As can be seen in Fig. 7, the absorption fraction and utilization index for the reaction scenaria are higher in the small channel compared to the large one which is attributed to the larger interfacial area (Table 1). The opposite, however, is seen for the physical absorption scenaria. This is because in the small channel the interfacial area of the bubble caps is much smaller than in the 0.5 mm channel. When there is only physical absorption, the interfacial mass transfer through the bubble caps is more significant than that through the film because the film becomes saturated in CO_2. Because of that, the increase in interfacial area in the small channel at the film region does not contribute significantly to mass transfer. Although the longer slug (longer recirculation cycle) in the small channel helps the mass transfer (Section 3.2), the effect is limited. Therefore, better absorption fraction and liquid utilization are obtained in the large channel.

$k_L a$ decreases as channel size decreases probably because the film which becomes quickly saturated and does not further contribute to mass transfer is extended in the small channel. Although k_L from the bubble cap increases in the small channel the corresponding specific area is small and the $k_L a$ associated with the bubble cap does not contribute sufficiently to the overall mass transfer coefficient.

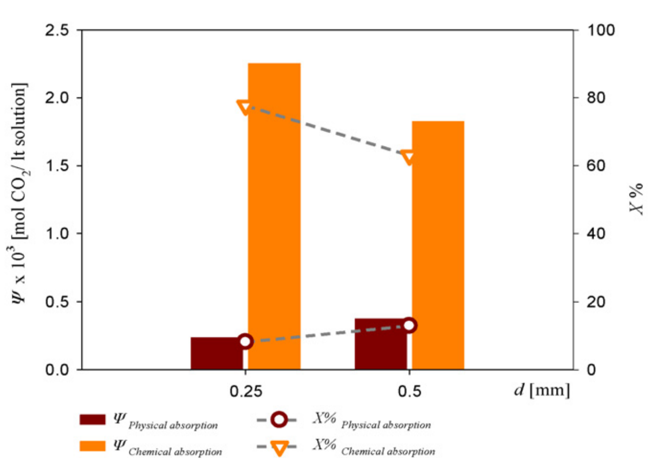

Fig. 7. Effect of channel dimension on liquid utilization index and CO_2 absorption fraction. $U_B = 0.05$ m/s, $\varepsilon_B = 0.554$, $V_{UC} = 0.196$ µl, $t = 0.05$ s.

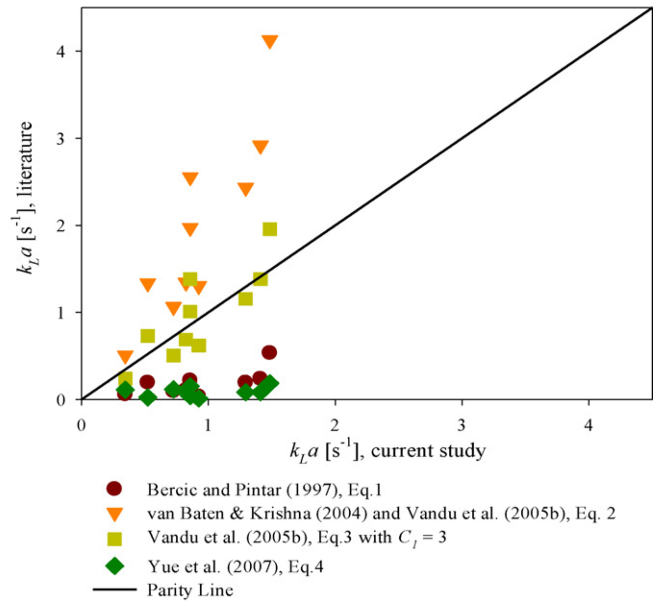

Fig. 8. Comparison of mass transfer coefficients calculated in this study against those predicted by literature correlations.

3.7. Comparisons of mass transfer parameters with literature

The mass transfer coefficients from the current simulations (see Table 1) are compared with those from literature correlations (Eqs. (1)–(4)) in Fig. 8. In general, $k_L a$ from this study fall within the predictions of literature correlations. Better agreement is seen with Eqs. (2) and (3). It is possible that higher $k_L a$ values were predicted by Eq. (2) compared to the current data because in this work narrow channels are used where the contribution of mass transfer from the bubble caps is not as significant as that from the film. When the mass transfer coefficient based only on the film size of the bubble is used, as in Eq. (3), the agreement is improved (see Fig. 8). Eq. (1) by Berčič and Pintar [13] underpredicts the mass transfer possibly because it was developed using long bubble lengths. Eq. (4) also underpredicts the current results probably because it was obtained at much higher gas and liquid velocities (10–300 times of those used in this study) [15]. The $k_L a$ from physical CO_2 absorption found here vary from 0.3 to 1.5 s^{-1} and the specific areas vary from 1000 to 7500 m^2/m^3. These values are within the range reported by Yue et al. [15] for similar gas–liquid contactors, i.e. $k_L a$ from 0.3 to 21 s^{-1} and a from 3400 to 9000 m^2/m^3, and outperform other contactors (see Table 2 in [15]).

The enhancement factors at $t = 0.05$ s for all the cases studied here are calculated using Eq. (23) and the results are shown in Table 1. With the presence of chemical reaction, CO_2 absorption improves by 3–12 fold.

4. Conclusions

The effects of bubble velocity, bubble geometry and channel dimension on the mass transfer performance of a Taylor flow microreactor for CO_2 absorption in a NaOH aqueous solution were studied numerically in the presence and absence of reaction. The reactor performance was evaluated using the

CO_2 absorption fraction $X\%$, the liquid utilization index Ψ, the mass transfer coefficient in the case of physical absorption and the mass transfer enhancement factor when a chemical reaction is present.

CO_2 absorption was found to be significantly higher when reaction was present than when there was no reaction because the transferred CO_2 was consumed which led to a constantly large driving force across the interface for mass transfer. The simulation results showed that the CO_2 absorption fraction increased with increasing bubble velocity and slug length, while it decreased with increasing bubble length and unit cell length. Interestingly, decreasing the channel size improved CO_2 absorption fraction for the reaction scenaria but decreased it in the physical absorption scenaria. The effects of bubble velocity and slug length were relatively small while generally the effects on $X\%$ of the above parameters were more significant in the physical absorption cases.

Together with CO_2 absorption, the amount of gas and/or liquid present affects the liquid utilization index Ψ. Similar to $X\%$, Ψ was found to be higher in the reaction cases than in the physical absorption ones. When there was reaction, Ψ was found to increase with increasing bubble velocity and bubble length, and with decreasing slug length, unit cell length and channel dimension. The effect of bubble and slug length was significant. With physical absorption, the effects of various parameters were found to be more moderate. Results showed that Ψ increased with increasing bubble velocity, bubble length and channel dimension and decreasing slug length and unit cell length.

The mass transfer coefficients in this study were found to be between 0.3 and 1.5 s^{-1}, in line with literature values for Taylor flow but higher than in normal gas–liquid contactors. The enhancement factor of chemical over physical absorption varied between 3 and 12. Enhancement was more significant at low bubble velocity, long bubble length, short unit cell length and small channel dimension.

The above suggest that it is important to establish bubble and slug lengths in a Taylor flow reactor that improve mass transfer through appropriate inlet configuration.

References

[1] K.A. Triplett, S.M. Ghiaasiaan, S.I. Abdel-Khalik, D.L. Sadowski, Gas–liquid two-phase flow in microchannels. Part I. Two-phase flow patterns, Int. J. Multiphase Flow 25 (1999) 377–394.

[2] I. Hassan, M. Vaillancourt, K. Pehlivan, Two-phase flow regime transitions in microchannels: a comparative experimental study, Microscale Thermophys. Eng. 9 (2005) 165–182.

[3] N. Shao, A. Gavriilidis, P. Angeli, Effect of inlet conditions on gas–liquid flow regimes in microchannels, in: Proceedings of the 1st International Conference on Microfluidics, Bologna, Italy, December 10–12, 2009.

[4] C.O. Vandu, J. Ellenberger, R. Krishna, Hydrodynamics and mass transfer in an upflow monolith loop reactor, Chem. Eng. Process. 44 (2005) 363–374.

[5] J.M. van Baten, R. Krishna, CFD simulations of mass transfer from Taylor bubbles rising in circular capillaries, Chem. Eng. Sci. 59 (2004) 2535–2545.

[6] A. Gunther, M. Jhunjhunwala, M. Thalmann, M.A. Schmidt, K.F. Jensen, Micromixing of miscible liquids in segmented gas–liquid flow, Langmuir 21 (2005) 1547–1555.

[7] W. Salman, A. Gavriilidis, P. Angeli, A model for predicting axial mixing during gas–liquid Taylor flow in microchannels at low Bodenstein numbers, Chem. Eng. J. 101 (2004) 391–396.

[8] M.T. Kreutzer, F. Kapteijn, J.A. Moulijn, Multiphase monolith reactors: chemical reaction engineering of segmented flow in microchannels, Chem. Eng. Sci. 60 (22) (2005) 5895–5916.

[9] P. Garstecki, M.J. Fuerstman, H.A. Stone, G.M. Whitesides, Formation of droplets and bubbles in a microfluidic T-junction—scaling and mechanism of break-up, Lab Chip 6 (2006) 437–446.

[10] V. Haverkamp, V. Hessel, H. Löwe, G. Menges, M.J.F. Warnier, E.V. Rebrow, M.H.J.M. de Croon, J.C. Schouten, M.A. Liauw, Hydrodynamics and mixer-induced bubble formation in micro bubble columns with single and multiple-channels, Chem. Eng. Technol. 29 (2006) 1015–1026.

[11] S. Irandoust, S. Ertle, B. Andersson, Gas–liquid mass transfer of Taylor flow through a capillary, Can. J. Chem. Eng. 70 (1992) 115.

[12] R. Clift, J.R. Grace, M.E. Weber, Bubbles, Drops and Particles, Academic Press, New York, 1978.

[13] G. Berčič, A. Pintar, Role of gas bubbles and liquid slug lengths on mass transport in the Taylor flow through capillaries, Chem. Eng. Sci. 52 (1997) 3709–3719.

[14] C.O. Vandu, H. Liu, R. Krishna, Mass transfer from Taylor bubbles rising in single capillaries, Chem. Eng. Process. 60 (2005) 6430–6437.

[15] J. Yue, G. Chen, Q. Yuan, L. Luo, Y. Gonthier, Hydrodynamics and mass transfer characteristics in gas–liquid flow through a rectangular microchannel, Chem. Eng. Sci. 62 (2007) 2096–2108.

[16] R.J. Farrauto, C.H. Bartholomew, Fundamentals of Industrial Catalytic Processes, Blackie Academic & Professional, London, 1997.

[17] S. Freguia, G.T. Rochelle, Modelling of CO_2 capture by aqueous monoethanolamine, AIChE J. 49 (2003) 1676–1686.

[18] A. Aroonwilas, A. Veawab, P. Tontiwachwuthikul, Behaviour of the mass transfer coefficient of structured packings in CO_2 absorbers with chemical reactions, Ind. Eng. Chem. Res. 38 (1999) 2044–2050.

[19] T. Taha, Z.F. Cui, CFD modelling of slug flow inside square capillaries, Chem. Eng. Sci. 61 (2006) 665–675.

[20] T. Taha, Z.F. Cui, CFD modelling of slug flow vertical tubes, Chem. Eng. Sci. 61 (2006) 676–687.

[21] D. Qian, A. Lawal, Numerical study on gas and liquid slugs for Taylor flow in a T-junction microchannel, Chem. Eng. Sci. 61 (2006) 7609–7625.

[22] N. Shao, W. Salman, A. Gavriilidis, P. Angeli, CFD simulations of the effect of inlet conditions on Taylor flow formation, Int. J. Heat Fluid Flow 29 (2008) 1603–1611.

[23] J.M. van Baten, R. Krishna, CFD simulations of wall mass transfer for Taylor flow in circular capillaries, Chem. Eng. Sci. 60 (2005) 1117–1126.

[24] P.V. Danckwerts, Gas–liquid Reactions, McGraw-Hill, New York, 1970.

[25] A. Schumpe, The estimation of gas solubilities in salt solutions, Chem. Eng. Sci. 48 (1993) 153–158.

[26] R. Pohorecki, W. Moniuk, Kinetics of reaction between carbon dioxide and hydroxyl ions in aqueous electrolyte solutions, Chem. Eng. Sci. 43 (1988) 1677–1684.

[27] G. Astarita, Mass Transfer with Chemical Reaction, Elsevier, New York, 1967.

[28] M. Zanfir, A. Gavriilidis, Ch. Wille, V. Hessel, Carbon dioxide absorption in a falling film microstructured reactor: experiments and modeling, Ind. Eng. Chem. Res. 44 (2005) 1742–1751.

[29] F.P. Bretherton, The motion of long bubbles in tubes, J. Fluid Mech. 10 (1961) 166–188.

[30] H. Liu, C.O. Vandu, R. Krishna, Hydrodynamics of Taylor flow in vertical capillaries: flow regimes, bubble rise velocity, liquid slug length, and pressure drop, Ind. Eng. Chem. Res. 44 (2005) 4884–4897.

[31] P. Aussilous, D. Quéré, Quick deposition of a fluid on the wall of a tube, Phys. Fluids 12 (10) (2000) 2367–2371.

[32] N. Shao, A. Gavriilidis, P. Angeli, Effect of inlet conditions on Taylor bubble length in microchannels. To be Presented in 2nd Micro and Nano Flows Conference, West London, UK, September 1–2, 2009.